energies

MDPI

Article

Large Scale Spectral Splitting Concentrator Photovoltaic System Based on Double Flat Waveguides

Ngoc Hai Vu [1,*], Thanh Tuan Pham [2,3] and Seoyong Shin [2,*]

[1] Faculty of Electrical and Electronics Engineering, Phenikaa University, Yen Nghia, Ha-Dong District, Hanoi 12116, Vietnam
[2] Department of Information and Communication Engineering, Myongji University, 116 Myongji-ro, Cheoin-gu, Yongin, Gyeonggi-do 17058, Korea; tuanpt@hcmute.edu.vn
[3] Renewable Energy Department, Faculty of Vehicle and Energy, HCMC University of Technology and Education, No. 1 Vo Van Ngan Street, Linh Chieu Ward, Thu Duc District, Ho Chi Minh City 700000, Vietnam
* Correspondence: hai.vungoc@phenikaa-uni.edu.vn (N.H.V.); sshin@mju.ac.kr (S.S.)

Received: 8 April 2020; Accepted: 6 May 2020; Published: 9 May 2020

Abstract: In this research, we present a novel design for a large scale spectral splitting concentrator photovoltaic system based on double flat waveguides. The sunlight concentrator consists of a Fresnel lens array and double waveguides. Sunlight is firstly concentrated by Fresnel lenses then reaches an upper flat waveguide (UFW). The dichroic mirror-coated prisms are positioned at each focused area to divide the sunlight spectrum into two bands. The mid-energy (mid E) band is reflected at the prism surface and coupled to the UFW. The GaInP/GaAs dual-junction solar cell is attached at the exit port of the UFW to maximize the electrical conversion efficiency of the mid E band. The low-energy (low E) band is transmitted and reaches a bottom flat waveguide (BFW). The mirror coated prisms are utilized to redirect the mid E band sunlight for coupling with the BFW. The GaInAsP/GaInAs dual-junction solar cell is applied to convert the low E band to electricity. The system was modeled using the commercial optic simulation software LightTools™. The results show that the proposed system can achieve optical efficiencies of 84.02% and 80.01% for the mid E band and low E band, respectively, and a 46.1% electrical conversion efficiency for the total system. The simulation of the system performance and comparison with other PV systems prove that our proposed design is a new approach for a highly efficient photovoltaic system.

Keywords: spectral splitting CPV; geometric optical design; photovoltaic; solar energy

1. Introduction

Solar is considered to be a promising renewable energy source, which can be a solution to the issues associated with fossil fuels and nuclear energy. Today, there are two main methods of harvesting sunlight and delivering useful energy: solar thermal and photovoltaic (PV) technologies [1]. Solar thermal technology converts solar radiation to useful heat, while PV technology transforms sunlight to electricity directly. Although thermal technology is cheaper than solar PV, the drawbacks are the low efficiency and difficulties in heat storage systems. When the solar PV system was first recognized as a promising renewable energy technology, many governments and research groups promoted research to improve the performance of PV systems. Recently, a very high electricity conversion efficiency of 46.0% in laboratory conditions was obtained by using multi-junction (MJ) solar cells [2]. However, the very high fabrication cost of multi-junction solar cells is a challenge for commercialization.

A concentrating photovoltaic (CPV) system is a promising solution in utilizing MJ solar cells for high efficiency solar energy systems [3]. In a CPV system, sunlight is focused by optical devices, then a small piece of solar cell is placed at the focal area to harvest the concentrated sunlight. In this way, the usage of expensive PV material is decreased significantly because of the replacement with more affordable mirrors and/or lenses [4]. In order to increase the electricity conversion efficiency, MJ solar cells are used in most CPV systems, and the high concentration ratio will offset their expensive cost [3]. Nevertheless, finding a solution for further increasing the efficiency and reducing the cost of PV systems is always of great interest. In spectral splitting CPV technology, sunlight is concentrated and separated into several wavelength bands by a spectral beam splitter, then solar cells with suitable band gaps are paired with each wavelength band to optimize the photoelectric conversion efficiency. Spectral splitting CPV technology has more potential applications [5]. In the literature, Jackson suggested the concept of a solar energy system based on splitting the solar spectrum and using a suitable convertor for each wavelength band for the first time in 1955 [1,6]. This approach is still applied extensively to solve spectral mismatch problems in solar cells. Many types of spectral splitting CPV system using different mechanisms have been developed up to now [1,7–13]. However, solar systems using spectral splitting technology have higher costs than conventional PV systems [5]. To achieve commercially viable competitive costs, the system cost should be offset by efficiency gains and the enlarging of system scales.

Traditionally, spectral splitting CPV systems have been implemented only on a small scale [1,5]. To increase system scale, large numbers of individual spectral splitting concentrator modules are gathered together and share the same sun tracking system. In a spectral splitting CPV system, focused beam handling part is quite complex. It includes a spectral splitter, secondary optics for the uniform distribution of the focused beam, solar cells, and a heat dissipation part. In this paper, an alternative approach is proposed for large scale spectral splitting CPV systems by replacing the focused beam handling part by double flat waveguides to eliminate secondary optics and share the solar cell and heat dissipater. The utilization of a waveguide as a solar concentrator has been reported in some research articles recently and attracted a lot of attention because this mechanism yields a compact, efficient, and light weight CPV system with a uniform flux distribution [14–24]. Waveguides using these CPV systems are classified in two main classes, namely, a lossless mechanism using stepped thickness waveguides [14,16,18] and a lossy mechanism using flat waveguides [17,19,20]. Moore et al. [14] proposed a concept of a lossless system based on a kind of planar solar concentrator with a "stepped-shape". Figure 1a shows the mechanism of the lossless structure. A lens array is used to concentrate sunlight, and the focused sunlight is coupled to a waveguide using light directing facets (inclined mirror, in most cases) then propagates to the end of waveguide by total internal reflection inside and exits from one edge of waveguide where the solar cell is placed. The waveguide thickness needs to be increased with subsequent lenses to avoid optical loss due to the interaction of the guiding ray with other light directing facets. Therefore, the geometrical concentration ratio of the system, which is the ratio of lens array area and output area, is limited. Enlarging the system scale does not increase the concentration ratio. In the lossy mechanism [25], the sunlight is focused by a lens array then coupled to a flat waveguide using a redirecting structure located at each focal point of the lens as shown in Figure 1b. The flat waveguide concentrator consists of three parts: a lens array, flat waveguide, and light-directing mirror. Because the thickness of waveguide does not change, the concentration ratio increases with an increase in the system scale. In the lossy structure, some of concentrated sunlight strikes and decouples with the redirecting structure when it propagates inside the waveguide; this is the cause of optical loss. Both structures have their own advantages and disadvantages; the lossless system has lower optical loss while the lossy system can achieve a much higher concentration ratio. The use of a waveguide as a solar concentrator for spectral splitting CPV systems is a promising new idea for the commercialization of solar energy systems with very high efficiency. The first study related to this idea was proposed by Ma et al. in 2014 [26]. They suggested a structure based on a double stepped thickness waveguide as a solar concentrator. Figure 1c shows the mechanism of Ma's approach.

A cylindrical micro-lens array focuses sunlight into double vertically staggered light guide layers. The redirecting structure in the upper waveguide is dichroic mirrors, which allow high reflectance for the middle energy (mid E) band of the solar spectrum ($\lambda < 850$ nm) and transmittance of the low energy (low E) band ($\lambda > 850$ nm) to the bottom waveguide. The mid E band propagates inside the upper waveguide and be absorbed by mid E band solar cells placed at the exit port. Similarly, the low E band is confined in the bottom waveguide and absorbed by a low E band solar cell. This design can achieve high optical efficiency, but it is for small scales, and the concentration ratio is low because of the use of cylindrical lens and the lossless mechanism.

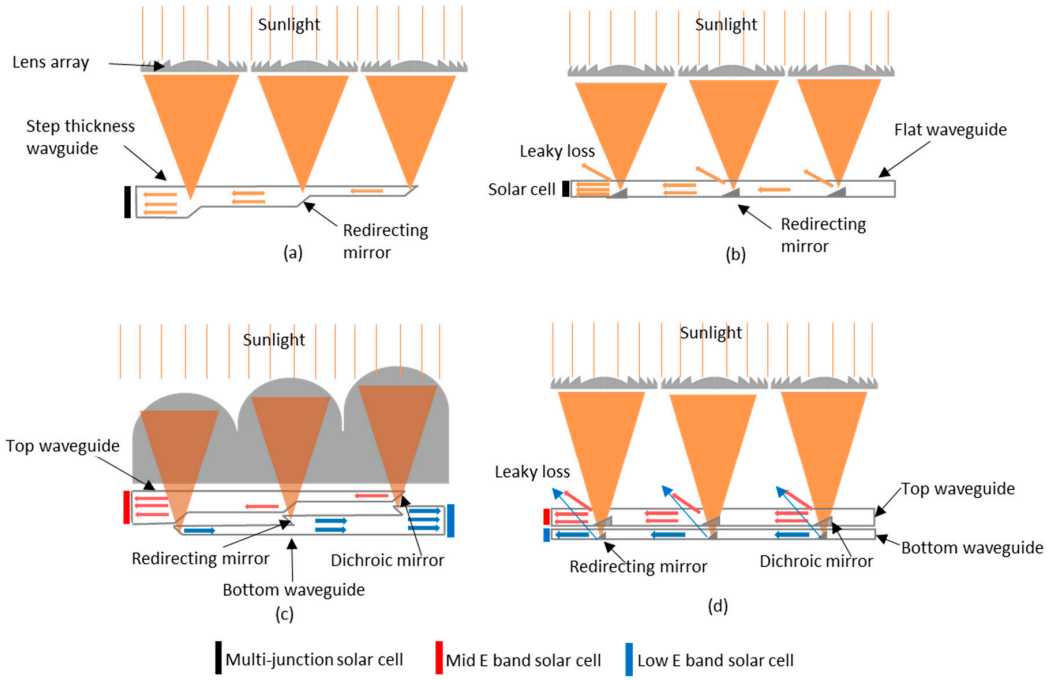

Figure 1. Concentrating photovoltaic (CPV) system based on waveguides: (**a**) lossless structure and (**b**) lossy structure. Spectral splitting CPV system based on double waveguide: (**c**) stepped thickness waveguide and (**d**) our proposed double flat waveguide.

Our goal is to propose a design for a large-scale spectral splitting CPV system whose structure is simple with a high geometrical concentration ratio and low fabrication cost by utilizing the double flat waveguide mechanism (lossy). The physical layout of our proposed spectral splitting CPV system approach is shown in Figure 1d. Sunlight focused by a Fresnel lens array reaches the upper flat waveguide (UFW) first, then strikes redirecting structures. The directing structures on the UFW are prisms with a dichroic mirror coating on the inclined surfaces. The mid E band of the solar spectrum is reflected and propagates inside the UFW; the low E band is transmitted to the bottom flat waveguide (BFW) and coupled inside by redirecting mirror coated prisms. The detail of the proposed design is described in Section 2. Theoretical analysis of the impact of design parameters on the system's performance is also discussed in this part. In Section 3, the proposed spectral splitting CPV system based on double waveguides is modeled in LightTools™ (Synopsys Inc., Mountain View, CA, USA) [27] to calculate the optical efficiency's dependence on some main parameters and evaluate the system's performance. Finally, Section 4 presents some conclusions and recommendations about the possibilities for future work.

2. Spectral Splitting Concentrator Photovoltaic System Concept

Beyond conventional solar concentrators, the main objective of the presented system is to separate the solar spectrum into two bands; each band is coupled and confined to one waveguide. At the

exit port of each waveguide, we place corresponding wavelength-sensitive solar cells for each band. The system is equipped with a sun-tracking device to collect normal direct sunlight. As shown in Figure 2, our proposed system is composed of two entities: a focusing lens array based on a Fresnel lens and double waveguides with suitable solar cells. The details of the optical system and design parameters are explained below.

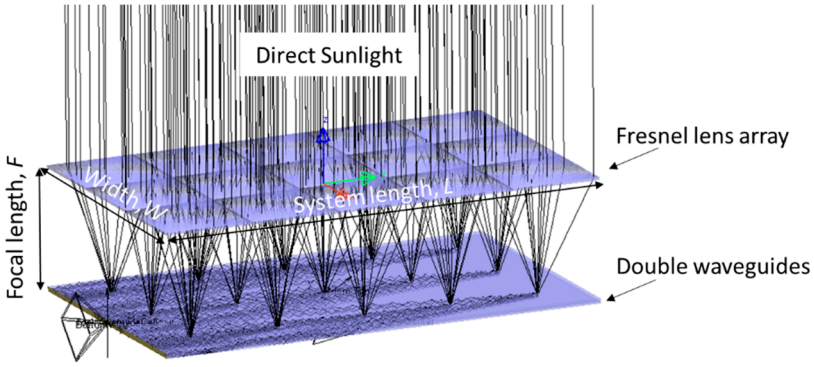

Figure 2. Physical layout of spectral splitting CPV system using double flat waveguides.

2.1. Fresnel Lens Array

In a conventional CPV system, there are many types of primary concentrator such as glass lenses, reflective parabolic mirrors, compound parabolic concentrators, diffractive concentrators, etc., but the main aim of this research is to create a highly efficient large-scale spectral splitting CPV system, so the requirements for the primary concentrators should be that they are thin, lightweight, and low in price. In this study, we utilized a Fresnel lens as the primary concentrator. A Fresnel lens is a non-imaging optics device that is constructed by micro ring-shaped segments on the surface. Sunlight is focused on a small spot, but this device does not provide a sharp image-like conventional convex lens. To meet the requirements, the commercial Fresnel lens made by DiYPRO Co., Ltd. (Suwon, Korea) is employed [28]. The Fresnel lens specification is shown in Table 1.

Table 1. Fresnel lens technical specification from DiYPRO Co., Ltd.

Fresnel Parameters	
Size (length, width and thickness)	240 × 240 × 3.5 mm
Groove pitch	50 μm
Focal length, *F*	300 mm
Material	PMMA *

* PMMA: Poly-methyl methacrylate.

The primary concentrator is a 3 × 5 square array of Fresnel lenses so that the system length, *L*, is 1200 mm and the width, *W*, is 720 mm. For a large scale CPV system based on waveguides, the sunlight travels considerably longer distances inside the waveguide, so the material attenuation and decoupling loss become more significant. Increasing the system's length leads to reducing the system's efficiency. Most typical CPV systems can achieve an optical efficiency >80%. Thus, the requirement for the system's design is that the optical efficiency must be higher than 80%. This is why a system length, *L*, of 1200 mm is selected. A system of length larger than 1200 mm cannot achieve 80% system efficiency, which will be mentioned in Section 3. The main thickness of system is defined by the focal length of the Fresnel lens, F, which is 300 mm. One of inherent disadvantages of the Fresnel lens in comparison with a reflective concentrator is the dispersion of the solar spectrum. The dispersion causes a broadening of the focal area, and this leads to decreases in the optical efficiency and concentration ratio. For our proposed CPV system based on waveguides, the size of focal area is also an important design parameter for the directing surfaces and the waveguide's thicknesses, which will be discussed

in Section 2.2. We analyzed the dispersion of the solar spectrum in the range of 400–2500 nm using the LightTools™ software. Figure 3a,b illustrate how sunlight is focused and dispersed through the Fresnel lens array by using ray tracing analysis. There is a 3 × 5 array of focused light spots on the focal plane. The simulation shows that the diameter of the focused area was 3.78 mm for the single wavelength of 550 nm but was widened to 8 mm for the full spectrum of sunlight. The dispersion at the focal plane can be explained by the Fresnel lens principal of convergence and the wavelength's dependence on the refractive index.

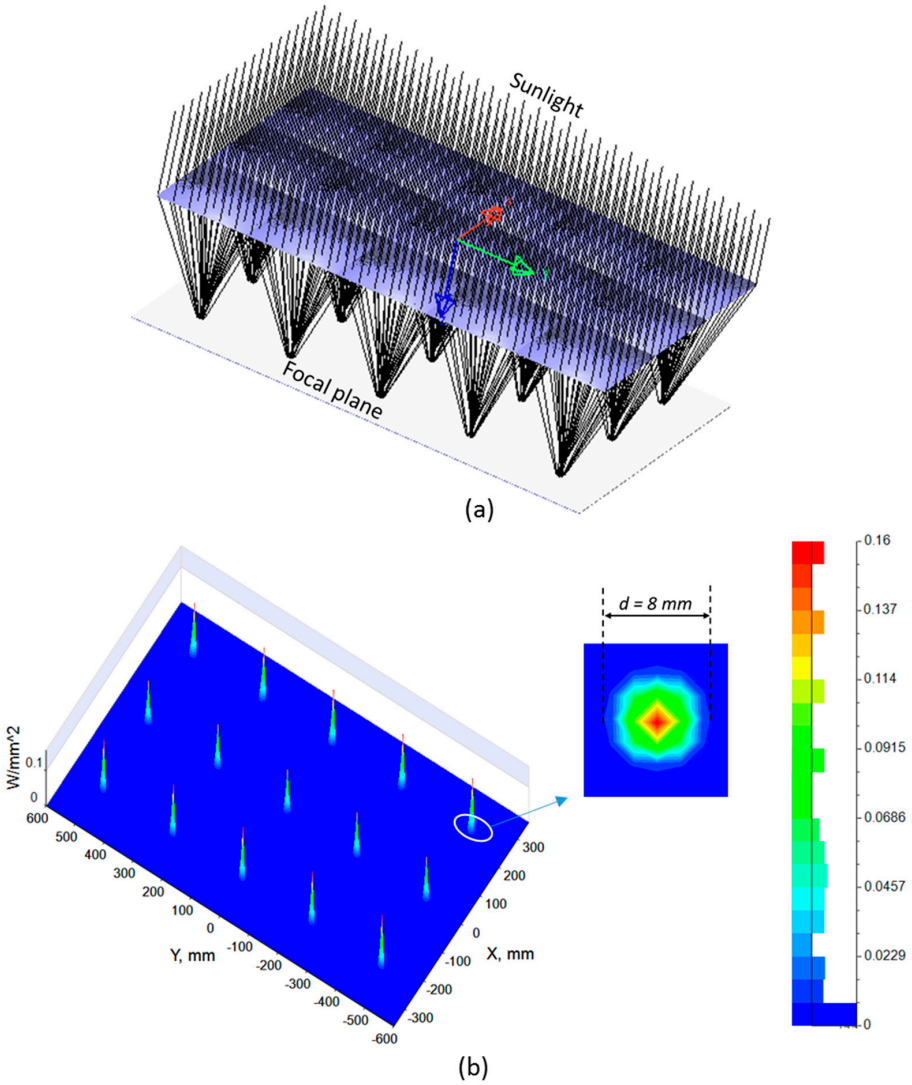

Figure 3. (**a**) The lens array distributes the concentrated sunlight on the focal plane; (**b**) The shape and the size of the concentrated sunlight on the focal plane.

2.2. Double Flat Waveguides

The planar waveguide concentrator was recently developed. In this approach, the concentrated beams are redirected inside the waveguide by injected facets and transferred to the exit port where a PV cell is attached. In our approach, double waveguides are utilized for the proposed spectral splitting CPV system. Figure 4 shows a side view and the ray tracing of our proposed system. The area around the focal point of the Fresnel lens is exaggerated for the illustration of the mechanism of coupling sunlight into double waveguides. The prism's side should be larger than the size of the concentrated light spot at its reflecting surface to cover all of the incident beam. Increasing the prism size leads

to decoupling loss in the system. Decoupling loss occurs when the sunlight propagates inside the waveguide and strikes other prisms then leaks out of the waveguide.

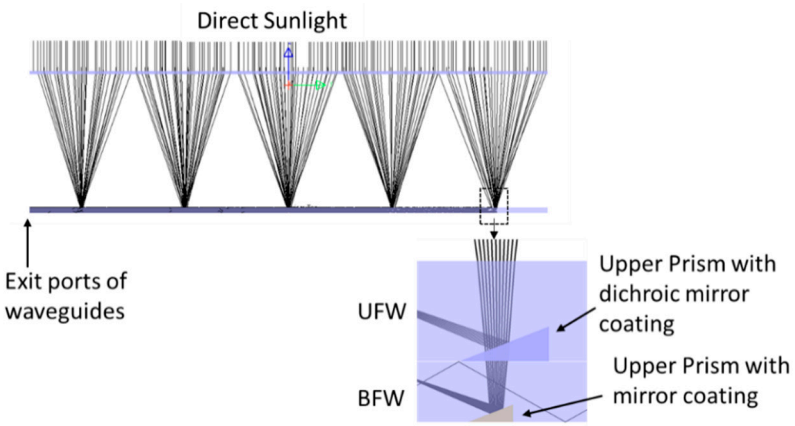

Figure 4. Details of double flat waveguides with an exaggeration at the position of redirecting prisms.

Firstly, the focused sunlight reaches the dichroic mirror coated prism (DMCP) in the UFW. The role of the DMCP is redirecting the focused beam, while concurrently acting as a spectral splitting facet. Only the mid E band of the solar spectrum is reflected and coupled to the UFW by total internal reflection (TIR). Therefore, the inclined angle of the prism should be designed to satisfy the TIR condition of the waveguide for the mid E light. One important parameter for calculating the inclined angle of the prism is the f-number of the Fresnel lens, which is the ratio of the focal length to the effective aperture diameter. In this research, the f-number of the Fresnel lens is 1.25. Based on this f-number, the angle of the focused beam is 43.6°. After refracting at the surface of the waveguide, this beam angle is reduced to 34.3°. The critical angle of the TIR condition inside the waveguide is 41.8°. Using this condition, we found out that an inclined angle for the prism of 30° can satisfy the requirement as shown in Figure 5a. If the f-number gets smaller then some of the light coming into focus are refracted too much and some edge rays do not satisfy the TIR condition. This calculation is based on a single wavelength of 550 nm with a refractive index of 1.49. There is the fact that this system operates across a wide range of the solar spectrum, so the material dispersion greatly affects the design of redirecting prism. It is very difficult to include this dispersion phenomenon in the calculation. In this research, we used simulation to reconfirm the prism design. By simulating the total system under the solar spectrum, by changing the incline angle and size of the prism, we can determine the appropriate design. The optimal design will provide the highest optical efficiency, which will be shown in Table 2.

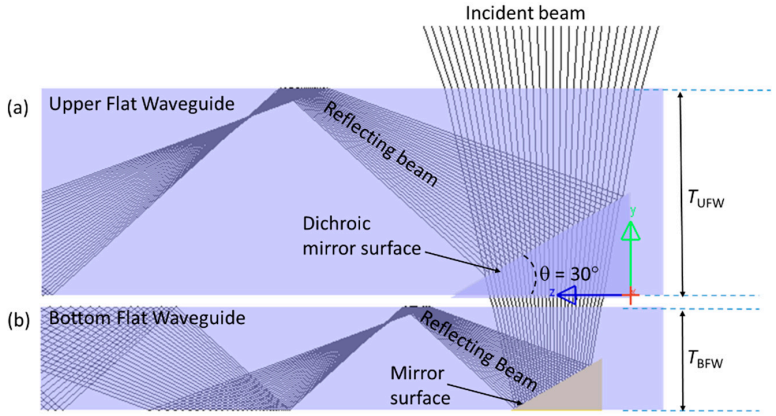

Figure 5. The design of redirecting mirrors in the: (**a**) upper flat waveguide (UFW) and (**b**) bottom flat waveguide (BFW).

Table 2. Some main parameters of double waveguides and system loss analysis.

Breakdown of Proposed Double Waveguide Parameters and Losses	
Upper Flat Waveguide (UFW)	
Prism's parameters (d_{UFW}/θ)	4.5 mm/30°
Prism's coating	Dichroic mirror
UFW's thickness, T_{UFW}	8 mm
Mid E band concentration ratio	150
Total Fresnel losses	9.48%
Dichroic mirror reflection loss	2.00%
Waveguide loss	5.30%
Total losses of mid E band	15.98%
Bottom Flat Waveguide (BFW)	
Prism's parameters (d_{BFW}/θ)	2.7 mm/30°
Prism's coating	Mirror
UFW's thickness, T_{BFW}	6 mm
Mid E band concentration ratio	200
Total Fresnel losses	14.10%
Dichroic mirror transmittance loss	3.11%
Waveguide loss	4.12%
Total losses of low E band	19.97%

After hitting the prism surface, the concentrated beam is separated into two bands by the dichroic beam splitter; the mid E band is reflected and coupled with the UFW, and the low E band is transmitted and reaches the BFW. Similar to the UFW, the prism structure is used to redirect and couple the low E band beam with the BFW. However, instead of the dichroic mirror, the reflecting mirror is applied on the prism surface as shown in Figure 5b.

The dichroic mirror is an important part of our proposed spectral splitting CPV system. Splitting the sunlight spectrum could be achieved by several optical elements such as prismatic elements, diffractive or holographic mirrors, luminescent materials, and thin film splitters. In this research, we focused on spectral splitting using thin film filters. Multilayer dichroic mirrors have surfaces with alternating thin film layers designed in such a way that interference effects can allow for complete transmission or complete reflection. The dichroic coating designed in our proposed system was a 66-layer TiO_2/SiO_2 coating. We used the LightTools™ software to evaluate the performance of the dichroic mirror, which we have calculated. We applied multiple layers of thin film to the single prism surface then set up the optical receivers to calculate the reflected beam power. A simulation was carried out with a solar spectrum from 400 to 2500 nm and rays with different angles of incidence (AOIs) ranging from 0° to 75°, with a step of 15°. Figure 6 shows the performance of the dichroic mirror designed with a cut-off wavelength at around 900–950 nm. This multilayer dichroic mirror design is applied to all redirecting prisms on the UFW for total system simulation. Based on this dichroic mirror, the appropriate solar cells are applied on the exit port of waveguide to optimize the electrical conversion efficiency. The types of solar cell will be discussed in Section 2.3.

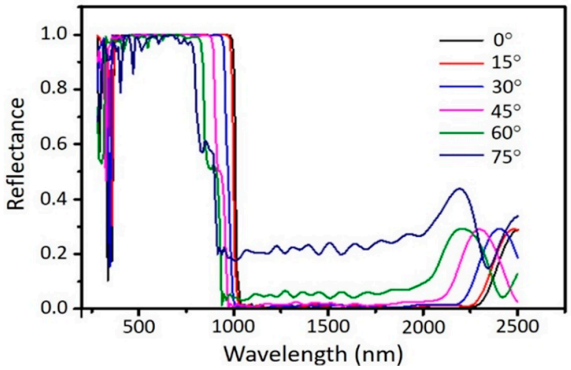

Figure 6. Simulation results on solar spectrum splitting by dichroic mirror with different angle off incident.

2.3. Exit Ports of Waveguides

Two types of dual junction solar cell were selected for this study: a low E band absorbing dual junction solar cell GaInAsP/GaInAs and mid E band absorbing dual junction solar cell GaInP/GaAs. The solar spectrum used in this research is generated by the LightTools™ software. It is divided into four bands, each band corresponding to a single junction solar cell, as shown in Figure 7a. Figure 7b shows that the mid E band solar cell attached on the exit port of the UFW is made of a GaInP top junction that has a band gap energy of 1.91 eV (649 nm) and a GaAs bottom junction that has a band gap energy of 1.42 eV (873 nm). The low E band solar cell attached on the BFW consists of a GaInAsP top junction that has a band gap energy of 0.98 eV (1265 nm) and a GaInAs bottom junction that has a band gap energy of 0.74 eV (1675 nm).

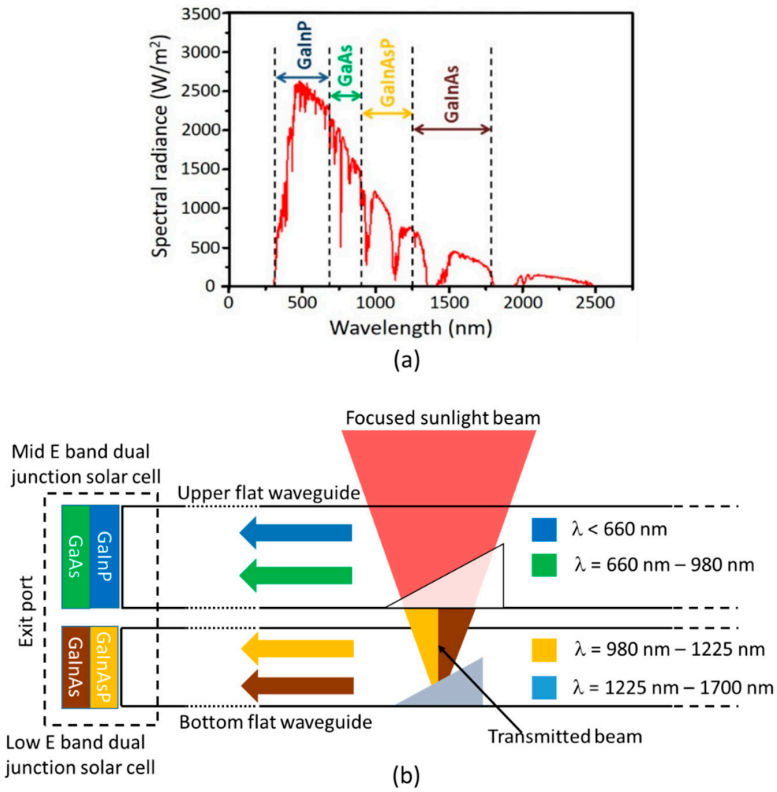

Figure 7. (**a**) Solar spectrum is divided into four bands corresponding to suitable solar cells. (**b**) Illustration of the solar cells at waveguide exit ports in association with other optical elements.

3. Simulation Results and Discussion

3.1. Optical Efficiency

The LightTools™ software was used to model our proposed spectral splitting CPV system. In order to propose a spectral splitting large scale system that is cost effective, the system design has to be compatible with larger scale mass production and industrial manufacturing processes. Thus, some main optical devices such as the Fresnel lens array, a flat waveguide that constitutes the system, should be made from thermal-plastic material. Poly-methyl methacrylate (PMMA) with a refractive index of 1.49 at a wavelength of 550 nm was set in the simulation. Because the refractive index is dependent on the wavelength of sunlight, the dispersion is important and must be included in the simulation. In the simulation model, sunlight with a wavelength ranging from 400 to 2500 nm was inserted as the source. The dispersion inside the total proposed system is taken into account by the LightTools software automatically. The redirecting prisms in the UFW and BFW should be made from glass because their surfaces need to be coated by dichroic films or mirrors. The interface between the waveguide/prism and waveguide/solar cell is filled by an optical epoxy as a matching gel with an index of 1.51. Figure 8a illustrates the simulation configuration of our design associated with the geometrical dimensions of the optical elements. Some representative rays are displayed to explain the loss mechanism inside the waveguides. A simulation for the optical performance of the proposed total system was implemented at real scale and under the full solar spectrum as shown in Figure 8b. An important property of the spectral splitting CPV system is based on the double waveguide; the geometrical concentration ratios for the mid E band and low E band are given by Equations (1) and (2), respectively.

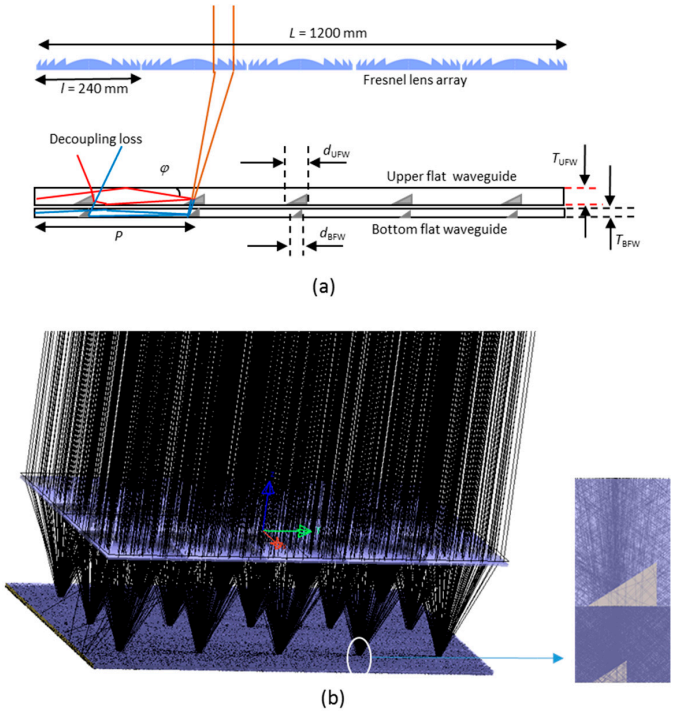

Figure 8. (**a**) Illustration of the simulation structure in association with geometrical parameters. Some representative rays are shown to explain the decoupling loss mechanism. (**b**) Simulation of the total system under the full solar spectrum with ray tracing.

$$C_{midEband} = \frac{Waveguide\ length}{UFW\ thickness} = \frac{L}{T_{UFW}} \quad (1)$$

$$C_{lowEband} = \frac{Waveguide\ length}{BFW\ thickness} = \frac{L}{T_{BFW}} \quad (2)$$

In our design, the length of system, L, is fixed at 1200 mm (five Fresnel lenses). Reducing the waveguide thicknesses can improve the concentration ratios. This will reduce the system cost because the expensive high efficiency solar cell area at the exit ports is reduced. However, there is a trade-off between the concentration ratio and optical efficiency, which will be discussed in Equations (3)–(6) and Figure 9.

The optical efficiency is defined by the ratio of output power at the exit port to the sunlight power. For the spectrum splitting CPV system, there are two optical efficiencies: the mid E band optical efficiency and low E band efficiency. The mid E band efficiency is the ratio of the output energy at the UFW to the mid E band energy of the input solar spectrum. Similarly, the low E band efficiency is the ratio of the output energy at the BFW to the low E band energy of the input solar spectrum. These optical efficiencies depend on many types of losses including Fresnel losses occurring at the interfaces of two different refractive index media, reflection or transmission losses in the mirror/dichroic-mirror coated surfaces of the redirecting prisms, decoupling loss inside the waveguide, and material absorption. When the sunlight propagates inside the waveguide, some of it hits prisms and leaks out; this is the cause of decoupling loss (Figure 8). Theoretical analysis for decoupling loss and material attenuation was proposed by Karp et al. in [25]. By applying Karp's waveguide loss theory in our case, the optical efficiencies for the UFW and BFW can be calculated by the combination of equations below:

$$\eta_{decouple}(P,\varphi) = \left(1 - \frac{1}{C_{UFW\ (or\ BFW)}}\right)^{\frac{P\tan\varphi}{2T}} \tag{3}$$

$$\eta_{position}(P,\varphi) = R \times \eta_{decouple} \times exp\left(\frac{-\alpha P}{\cos\varphi}\right) \tag{4}$$

$$\eta_{total} = \frac{\sum_P \int_0^{\varphi_{\max}} \eta_{postion}(P,\varphi)}{\frac{(2L-l)}{2l}}; P = \frac{l}{2}, \frac{3l}{2}, \frac{5l}{2}, \ldots, \frac{2L-l}{2l} \tag{5}$$

where $\eta_{decouple}$ is related to the decoupling losses; $\eta_{position}$ is related to the material attenuation, and η_{total} represents the total optical efficiency inside the waveguide. C_{UFW} and C_{BFW} are the concentration ratios of the Fresnel lens on the two waveguides, and they can be calculated by:

$$C_{UFW} = \left(\frac{l}{d_{UFW}}\right)^2;\ C_{UFW} = \left(\frac{l}{d_{BFW}}\right)^2 \tag{6}$$

A minimal prism size will increase these concentration ratios. However, the prisms must be large enough to cover all of the focused beam falling down on the inclined surfaces of the prisms in both the UFW and BFW. Using ray-tracing analysis, we can determine the minimal size of the prisms. In the simulation model, all parameters such as the Fresnel lens array and waveguide size were fixed, except for the size of prisms. We found that the output powers of the UFW and BFW do not change with $d_{UFW} > 4.5$ mm and $d_{BFW} > 2.7$ mm and decrease significantly when $d_{UFW} < 4.5$ mm and $d_{BFW} < 2.7$, respectively. This means that the appropriate sizes of prisms in the UFW and BFW are 4.5 mm and 2.7 mm, respectively.

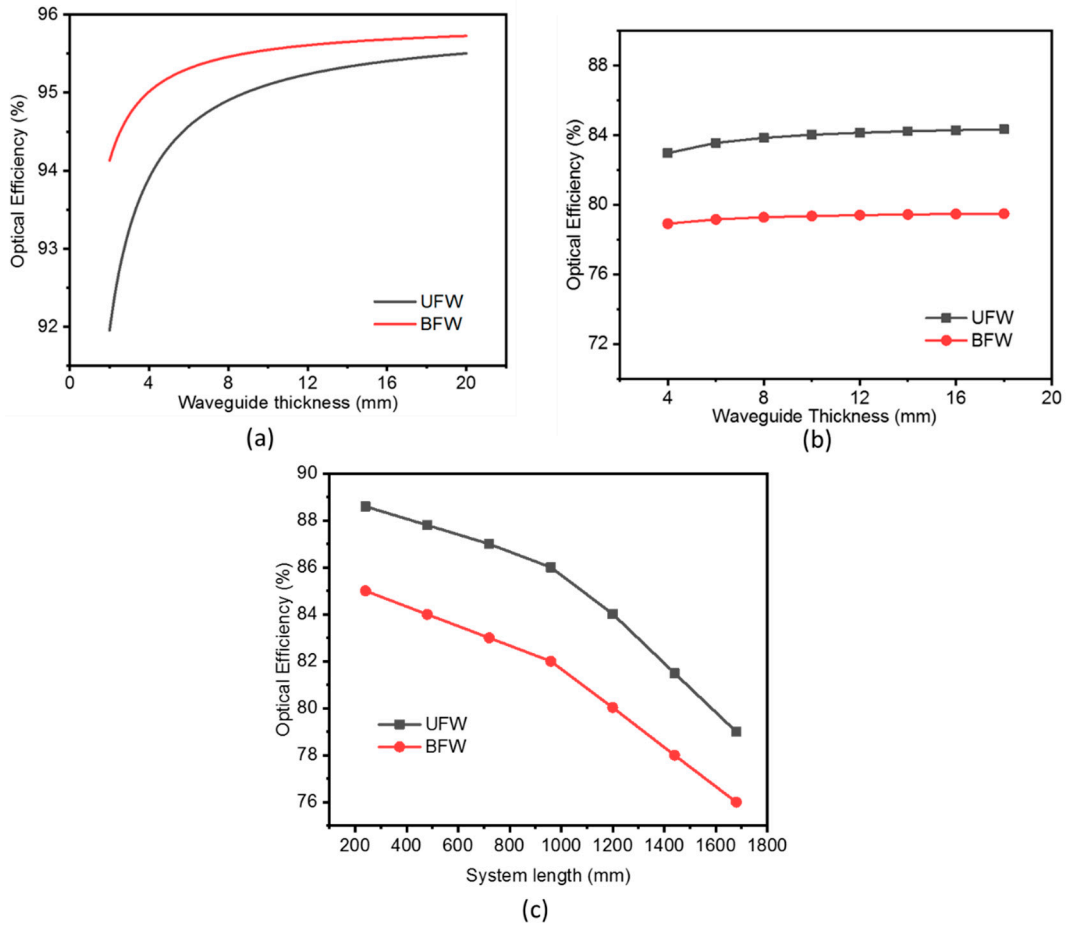

Figure 9. The dependence of optical efficiency on the waveguide thickness: (**a**) theoretical analysis for case of coupling angle (φ) = 30° and (**b**) simulation results. (**c**) Simulation result for the optical efficiency depends on system length.

As denoted in Figure 8, P is the distance from each prism to the exit port; T is the thickness of the waveguide (T_{UFW} and T_{BFW} are the thicknesses of the UFW and BFW, respectively); φ is the angle of the ray inside the waveguide; and α is the absorption coefficient. Equation (3) shows the optical efficiency from the input position, P; it expresses the probability of the ray being able to be transmitted to the exit port. Because the sizes of the prisms were fixed, $\eta_{decouple}$ is a function of the waveguide thickness. Increasing the waveguide thickness or decreasing the prism size will reduce the decoupling loss. Equation (4) is related to the material absorption, with exponential decay with an increasing path length of the ray. Taking the integration over all prism positions, Ps, and the coupling angle φ, in Equation (6) will determine in the total optical efficiency of the waveguides, η_{total}. Figure 9a plots the optical efficiency as a function of waveguide thickness in the case of fixed φ = 30°. It shows a qualitative understanding about the loss mechanism inside the waveguide, i.e., a thicker waveguide yields a higher efficiency. It is very complicated to calculate the optical loss based on theoretical equations because there are many loss mechanisms and material dispersions. However, theoretical analysis provides an understanding about the influence of physical factors on the optical loss of the system. To calculate the total optical efficiency, the total system was simulated using the LightTools software with the full solar spectrum. We have to take into account the entire cone of focused beam as well as the coupling angle. Additionally, the Fresnel losses at many surfaces are too complicated to predict by theory, but they significantly affect the system's optical efficiency. To evaluate the optical efficiency of the system, we carried out simulations with different waveguide thicknesses, T_{UFW} and T_{BFW}. Figure 9a shows that the loss inside the UFW is higher than the loss in the BFW because the prism size in the UFW is larger than that in the BFW. However, the total loss of the UFW is lower than of the

BFW because of Fresnel losses. To reach the BFW, the sunlight has to pass more intersection surfaces than to reach the UFW. Based on theoretical calculation and simulation, we selected the thicknesses of waveguides as T_{UFW} = 8 mm and T_{BFW} = 6 mm. One of the significant losses is the material attenuation of sunlight inside the waveguide. This loss limited the system length. To confirm that a system length of 1200 mm satisfied the requirement that the optical efficiency is not lower than 80%, we carried out the simulation of system with different lengths, L = 240 to 1680 mm in steps of 240 mm, corresponding to changing the number of Fresnel lenses across the length of the array from 1 to 7. The result in Figure 9c shows that L = 1200 mm is the critical point to achieve the requirement set in Section 2.1. To breakdown all the kinds of losses in our proposed system, we inserted optical receivers at many positions such as at the sunlight input area, at the exit ports of the two waveguides, and before and after boundaries where Fresnel losses occur. The optical loss analysis is shown in Table 2.

3.2. System Performance

One of the requirements for the proper operation of the system is that the sunlight should be perpendicular to the surface of Fresnel lens, then the focused beam should always be centered on the redirecting surfaces of the prisms. Because the sunlight direction changes over a day and a year, a sun tracking system needs to be utilized to maintain precise alignment between the system and sunlight direction. The required accuracy of the sun tracking system is very important for the operation of the system. This accuracy can be determined according to system's angular tolerance. The angular tolerance of the system is defined by the acceptable angular deviation of sunlight to the normal direction of the system surface. The acceptant angle of the system is the angular deviation that reduces efficiency by 10%. To calculate the acceptant angle, we do the simulation for the total system along the North–South (N–S) and East–West (E–W) axes, and slightly change the sunlight direction (Figure 10a). The simulation model is the same as in Section 3.1, but the incident angle of the sunlight beam changes. The dependence of the optical efficiency on sunlight angular deviation along the N–S and E–W axes was examined and is shown in Figure 10b. The simulation results show that the acceptance angle for the BFW is smaller than that for the UFW because of the difference in prism size. Based on Figure 10b, we can determine the acceptant angle of system to be ±0.5°. Many sun tracking systems have been proposed over the past 20 years in the literature. The range of tracking system accuracy is from 0.05° to 1° using closed-loop control mechanisms. Sun tracing with a higher accuracy is more expensive. The accuracy requirement of 0.5° of our proposed system is compatible with most typical, available sun tracking systems. With the increase in the size of the redirecting prisms, the focused light couples more effectively to the waveguides rather than the sun-tracking tolerance being increased. Lower accuracy sun tracking costs less; however, a larger prism size then reduces the optical efficiency (Equations (3)–(6)). Therefore, the tolerance and the optical efficiency should be kept in balance. It means that depending on real circumstances, with a given accuracy of solar tracking system, we can design a proper system that provides the highest optical efficiency.

To evaluate the system's performance over a day, we carried out simulations with the site of application at 127° longitude and 37.5° latitude. The GaInP/GaAs dual-junction solar cell is attached at the exit port of the UFW and the GaInAsP/GaInAs dual-junction solar cell is at the exit port of the BFW. The electrical conversion efficiency of the GaInP/GaAs dual-junction solar cells is 34.2% for the full solar spectrum corresponding with an in-band efficiency of 61.53% [23]. The in-band efficiency is the efficiency of solar cell operating under its appropriate solar spectrum band. The GaInAsP/GaInAs dual-junction solar cell has a conversion efficiency of 32.5% and an in-band efficiency of 43.9% [23]. The total electrical conversion efficiency of the system can be calculated by Equation (7).

$$\eta_{system} = \eta_{UFW}\eta_{GaInP/GaAs}\, k_{mid\ E\ band} + \eta_{BFW}\eta_{GaInAsP/GaInAs}\, k_{low\ E\ band} \quad (7)$$

where η_{system} is the total electrical conversion efficiency; η_{UFW} and η_{BFW} are the optical efficiencies of the double waveguides; $\eta_{GaInP/GaAs}$ and $\eta_{GaInAsP/GaInAs}$ are the in-band efficiencies of each solar cell

type; and $k_{mid\ E\ band}$ and $k_{low\ E\ band}$ are the ratios of the in-band energy over the total spectrum energy. Following Equation (7), the total electrical conversion efficiency of the system is 46.1%. The output power of the system, P_{system} can be calculated by Equation (8).

$$P_{system} = \eta_{system} \times Solar\ Irradiation \tag{8}$$

Figure 11 shows the output power at the UFW and BFW over time on a sunny day in summer. The total energy harvested on this day is 2.448 kWh. It can be calculated by taking the integral of the output power over the time for both the UFW and BFW.

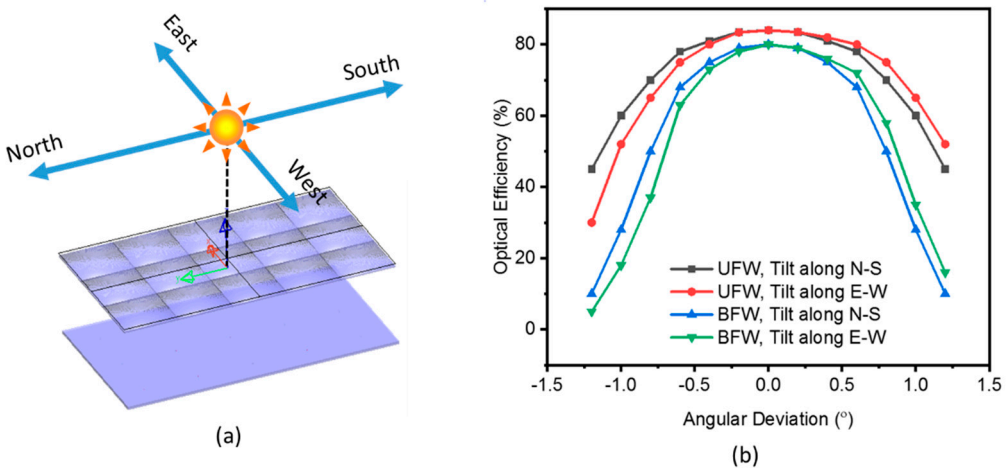

Figure 10. (**a**) The alignment of system along the North–South (N–S) and East–West (E–W) axes; (**b**) Variation of optical efficiency according to angular deviation along the N–S and E–W axes.

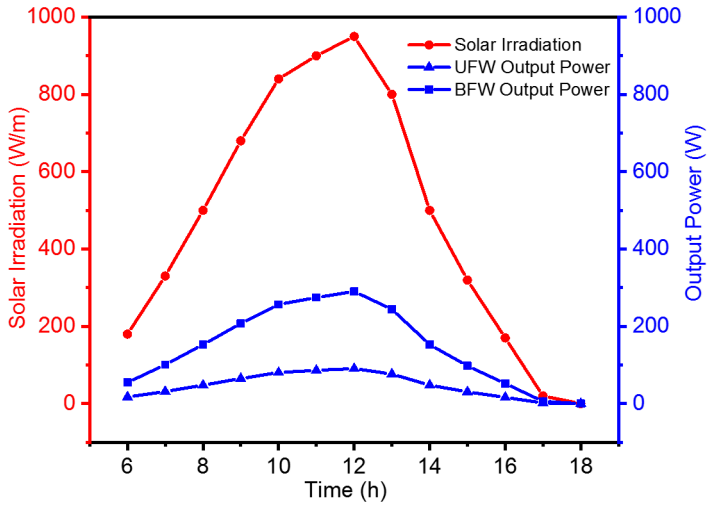

Figure 11. Solar irradiation and electrical output power of the UFW and BFW over time on a summer's day.

For the CPV system, not only the concentration ratio but also the optical efficiency affects the system's performance, but the irradiance uniformity of the concentrated sunlight on the surface of the solar cells is also important. For a typical CPV system including spectral splitting CPV, non-uniformity of the concentrated sunlight beam reduces solar cell electrical performance and lifetime [29]. High flux contrast on the cell's surface leads to resistance losses. In our proposed system, the double waveguides act as a homogenizer for achieving highly uniform irradiance on the solar cells.

Many types of spectral splitting CPV system have been developed with various approaches recently, but none of them have been commercialized because they are still too expensive in comparison

with typical CPVs. Additionally, most of approaches for spectral splitting CPV systems are at a small scale, thus it is difficult for them to be used widely. This research provides a new approach to increasing the system scale by using a waveguide mechanism. It shows great potential for commercialization. However, we need to carry out a performance evaluation of our proposed system in comparison with typical plat PVs and CPVs that have been commercialized. Due to variety of operating conditions, system comparison is not easy; however, we used the data from developers' publications in order to evaluate our proposed system. For comparison, we simulated the cases of flat PV and CPV based on the developers' parameters [30] and under the same climates as found in Seoul (Korea, where DNI is very low in winter) and Phoenix (Arizona state, United States, where DNI is high). We assumed that the collecting areas of the PV and CPV systems were the same with our proposed design. The comparison in Table 3 shows that the energy harvested per year in the low DNI area (Seoul) increases by only 21.1% by using our proposed system in comparison with using conventional PV. In the high DNI area, the energy harvested per year is improved significantly (207%). This shows that our proposed system has more advantage in areas where DNI is high.

Table 3. Comparison in performance between conventional photovoltaic (PV) systems, CPV systems, and our proposed design.

	Conventional PV	**Commercialized CPV**	**Our Proposed System**
Situation	Commercialized	Commercialized	Research
Type	Non-concentration	High concentration	High concentration
Optics for concentrator	None	Fresnel lenses	Fresnel lenses and Waveguides
Concentration ratio	0	~500	150 for Mid E band and 200 for Low E band
Sun tracking	None	Required	Required
Solar cell	Si solar cell with efficiency of 18–20%	Multi-junction cells GaInAsP/GaInAs with eff. of 35%	Two types of dual junction cell: GaInP/GaAs and GaInAsP/GaInAs
Energy harvesting on a summer's day	Simulation in ideal circumstances In Seoul: 1.05 kWh In Phoenix: 1.14 KWh	Simulation in ideal circumstances In Seoul: 1.44 kWh In Phoenix: 1.65 kWh	Simulation in ideal circumstances In Seoul: 2.488 kWh In Phoenix: 2.6 kWh
Energy harvesting per year	By simulation In Seoul: 184 KWh In Phoenix: 325.0 KWh	By simulation In Seoul: 154.5 kWh In Phoenix: 468 kWh	By simulation In Seoul: 223 KWh In Phoenix: 673.1 KWh

4. Conclusions

The proposed spectral splitting concentrator with a Fresnel lens array and double flat waveguide has been designed, modeled, and simulated for large scale application. The design concept allows two types of solar cell to be used with appropriate operational spectral bands, intending to maximize the electrical conversion efficiency. Theoretical analysis and system modeling have shown that the waveguide thicknesses and redirecting prism sizes are two important parameters that directly affect the system optical efficiency. Simulations of system performance were carried out for the evaluation of the optical losses and the energy harvested over a day and a year in different climates (high and low DNI). A high electrical conversion efficiency of 46% was achieved with a larger system scale of $1200 \times 720 \times 300$ mm. A comparison with conventional PV and CPV performances shows a great advantage of our design in high DNI climates. System prototype fabrication and experiments should be done in future research to verify the design concept and evaluate the commercial viability.

Author Contributions: Original idea conceptualization, N.H.V.; methodology, N.H.V.; Simulation, N.H.V. and T.T.P.; formal analysis, N.H.V.; writing-original draft preparation, N.H.V.; review and editing, S.S; project administration, S.S.; funding acquisition, S.S. All authors have read and agreed to the published version of the manuscript.

Funding: This research was funded by the Basic Science Research Program through the National Research Foundation of Korea (NRF) funded by the Ministry of Education (2017R1D1A1B03031338).

Conflicts of Interest: The authors declare no conflict of interest.

References

1. Mojiri, A.; Taylor, R.; Thomsen, E.; Rosengarten, G. Spectral beam splitting for efficient conversion of solar energy—A review. *Renew. Sustain. Energy Rev.* **2013**, *28*, 654–663. [CrossRef]
2. Green, M.A.; Hishikawa, Y.; Dunlop, E.D.; Levi, D.H.; Hohl-Ebinger, J.; Yoshita, M.; Ho-Baillie, A.W.Y. Solar cell efficiency tables (Version 53). *Prog. Photovolt. Res. Appl.* **2019**, *27*, 3–12. [CrossRef]
3. Buljan, M.; Mendes-Lopes, J.; Benítez, P.; Miñano, J.C. Recent trends in concentrated photovoltaics concentrators' architecture. *J. Photonics Energy* **2014**, *4*, 040995. [CrossRef]
4. Shanks, K.; Senthilarasu, S.; Mallick, T.K. Optics for concentrating photovoltaics: Trends, limits and opportunities for materials and design. *Renew. Sustain. Energy Rev.* **2016**, *60*, 394–407. [CrossRef]
5. Imenes, A.G.; Mills, D.R. Spectral beam splitting technology for increased conversion efficiency in solar concentrating systems: A review. *Sol. Energy Mater. Sol. Cells* **2004**, *84*, 19–69. [CrossRef]
6. Jackson, E.D. Areas for improvement of the semiconductor solar energy converter. In Proceedings of the Trans. Intern. Conf. on the Use of Solar Energy-The Scientific Basis, Tucson, AZ, USA, 31 October 1955; p. 122.
7. Rand, B.P.; Genoe, J.; Heremans, P.; Poortmans, J. Solar Cells Utilizing Small Molecular Weight Organic Semiconductors. *Prog. Photovolt. Res. Appl.* **2007**, *15*, 659–676. [CrossRef]
8. Goldschmidt, J.C.; Do, C.; Peters, M.; Goetzberger, A. Spectral splitting module geometry that utilizes light trapping. *Sol. Energy Mater. Sol. Cells* **2013**, *108*, 57–64. [CrossRef]
9. Xiong, K.; Lu, S.; Dong, J.; Zhou, T.; Jiang, D.; Wang, R.; Yang, H. Light-splitting photovoltaic system utilizing two dual-junction solar cells. *Sol. Energy* **2010**, *84*, 1975–1978. [CrossRef]
10. Zhao, Y.; Sheng, M.-Y.; Zhou, W.-X.; Shen, Y.; Hu, E.-T.; Chen, J.-B.; Xu, M.; Zheng, Y.-X.; Lee, Y.-P.; Lynch, D.W.; et al. A solar photovoltaic system with ideal efficiency close to the theoretical limit. *Opt. Express* **2012**, *20*, A28. [CrossRef]
11. Imenes, A.G.; Buie, D.; McKenzie, D. The design of broadband, wide-angle interference filters for solar concentrating systems. *Sol. Energy Mater. Sol. Cells* **2006**, *90*, 1579–1606. [CrossRef]
12. Peters, M.; Goldschmidt, J.C.; Löper, P.; Groß, B.; Üpping, J.; Dimroth, F.; Wehrspohn, R.B.; Blasi, B. Spectrally-Selective photonic structures for PV applications. *Energies* **2010**, *3*, 171–193. [CrossRef]
13. Kostuk, R.K.; Rosenberg, G. Analysis and design of holographic solar concentrators. *High Low Conc. Sol. Electr. Appl. III* **2008**, *7043*, 70430I.
14. Moore, D.; Schmidt, G.; Unger, B. Concentrated photovoltaics stepped planar light guide. In Proceedings of the International Optical Design Conference, Jackson Hole, WY, USA, 13–17 June 2010; Volume 7652.
15. Vu, N.H.; Shin, S. A concentrator photovoltaic system based on a combination of prism-compound parabolic concentrators. *Energies* **2016**, *9*, 645. [CrossRef]
16. Vu, N.; Shin, S. A Large Scale Daylighting System Based on a Stepped Thickness Waveguide. *Energies* **2016**, *9*, 71. [CrossRef]
17. Bouchard, S.; Thibault, S. GRIN planar waveguide concentrator used with a single axis tracker. *Opt. Express* **2014**, *22*, A248–A258. [CrossRef] [PubMed]
18. Vu, N.H.; Shin, S. Optical fiber daylighting system combined with LED lighting and CPV based on stepped thickness waveguide for indoor lighting. *J. Opt. Soc. Korea* **2016**, *20*, 488–499. [CrossRef]
19. Teng, T.-C.; Lai, W.-C. Planar solar concentrator featuring alignment-free total-internal-reflection collectors and an innovative compound tracker. *Opt. Express* **2014**, *22*, A1818. [CrossRef]
20. Bouchard, S.; Thibault, S. Planar waveguide concentrator used with a seasonal tracker. *Appl. Opt.* **2012**, *51*, 6848. [CrossRef]
21. Wu, H.-Y.; Chu, S.-C. Ray-leakage-free sawtooth-shaped planar lightguide solar concentrators. *Opt. Express* **2013**, *21*, 20073. [CrossRef]

22. Baker, K.A.; Karp, J.H.; Tremblay, E.J.; Hallas, J.M.; Ford, J.E. Reactive self-tracking solar concentrators: Concept, design, and initial materials characterization. *Appl. Opt.* **2012**, *51*, 1086. [CrossRef]
23. Vu, N.H.; Pham, T.T.; Shin, S. Flat concentrator photovoltaic system for automotive applications. *Sol. Energy* **2019**, *190*, 246–254. [CrossRef]
24. Xie, P.; Lin, H.; Liu, Y.; Li, B. Total internal reflection-based planar waveguide solar concentrator with symmetric air prisms as couplers. *Opt. Express* **2014**, *22*, A1389. [CrossRef] [PubMed]
25. Karp, J.H.; Tremblay, E.J.; Ford, J.E. Planar micro-optic solar concentrator. *Opt. Express* **2010**, *18*, 1122–1133. [CrossRef] [PubMed]
26. Ma, H.; Meng, Q.; Xu, S.; Dong, J.; Li, W. High-integrated spectral splitting solar concentrator with double-light guide layers. *Opt. Eng.* **2014**, *53*, 105102. [CrossRef]
27. LightTools Illumination Design Software. Available online: https://www.synopsys.com/optical-solutions/lighttools.html (accessed on 12 March 2020).
28. DiYPRO Co., Ltd. Available online: https://diypro.en.ec21.com/ (accessed on 12 March 2020).
29. Paul, D.I.; Smyth, M.; Zacharopoulos, A.; Mondol, J. The effects of nonuniform illumination on the electrical performance of a single conventional photovoltaic cell. *Int. J. Photoenergy* **2015**, 1–10. [CrossRef]
30. Khamooshi, M.; Salati, H.; Egelioglu, F.; Hooshyar Faghiri, A.; Tarabishi, J.; Babadi, S. A review of solar photovoltaic concentrators. *Int. J. Photoenergy* **2014**, 1–17. [CrossRef]

© 2020 by the authors. Licensee MDPI, Basel, Switzerland. This article is an open access article distributed under the terms and conditions of the Creative Commons Attribution (CC BY) license (http://creativecommons.org/licenses/by/4.0/).